Excitation function and yield for the ^{103}Rh(d,2n)^{103}Pd nuclear reaction: optimization of the production of palladium-103

Simone Manenti[a,*], María del Carmen Alí Santoro[b], Giulio Cotogno[c], Charlotte Duchemin[d], Ferid Haddad[d,e], Uwe Holzwarth[c], Flavia Groppi[a]

[a] *LASA, Università degli Studi di Milano and INFN-Milano, via F.lli Cervi 201, I-20090 Segrate (MI), Italy*
[b] *Centro Atómico Ezeiza - Comisión Nacional de Energía Atómica, Presbítero Juan González y Aragón Nro.15 , Ezeiza, Buenos Aires, Argentina*
[c] *Institute for Health and Consumer Protection, Joint Research Centre, European Commission, TP 500, I-21020 Ispra (VA), Italy*
[d] *SUBATECH, Ecole des Mines de Nantes, Université de Nantes, CNRS/IN2P3, Nantes, France*
[e] *GIP Arronax, 1 rue Aronnax, 44817 Saint-Herblain, France*

Abstract

Deuteron-induced nuclear reactions for the generation of ^{103}Pd were investigated using the stacked-foil activation technique on rhodium targets at deuteron energies up to $E_d = 33$ MeV. The excitation functions of the reactions ^{103}Rh(d,xn)^{101,103}Pd, ^{103}Rh(d,x)^{100g,cum,101m,g,102m,g}Rh and ^{103}Rh(d,2p)^{103}Ru have been measured, and the Thick-Target Yield for ^{103}Pd has been calculated.

Keywords: palladium-103, ^{103}Pd, rhodium target, deuteron particle irradiation, cross-section, excitation function, yield, Pd, Rh, Ru radioisotopes, cyclotron

1. Introduction

^{103}Pd ($t_{1/2}$=16.991 d [1]) decays almost exclusively (99.90 %) by electron capture (EC) to ^{103m}Rh ($t_{1/2}$=56.12 min) which de-excites through internal transition (IT). As a result of these processes (EC and IT) Auger-electrons and

*Corresponding author +39 02 503 19528
Email addresses: simone.manenti@mi.infn.it (Simone Manenti), simone.manenti@gmail.com (Simone Manenti)

X-rays are emitted which are ideally suited for cancer therapy. Taking into account also the de-excitation of the "daughter" nuclide ^{103m}Rh, every 100 decays of ^{103}Pd are accompanied by the emission of about 263 Auger electrons, 188 low-energy conversion electrons and 97 X-rays [2]. These decay features and the practical absence of high-energy γ-rays make ^{103}Pd particulary suitable for interstitial brachytherapy: encapsulated in millimetre-size seed implants it is used in prostate [3], breast [4] or choroidal melanomas [5] cancer brachytherapy. It has been shown that gold nanoparticles (Au NPs) distributed in the vicinity of ^{103}Pd radioactive implants can act as radiosensitivers that strongly enhance the therapeutic dose of radioactive implants [6, 7]. A new strategy under development to replace millimetre-size seeds [8], consist in injecting radioactive nanoparticles in the affected tissues. The development of ^{103}Pd@Au NPs distributed in the diseased tissue, could increase the uniformity of the treatment compared to larger seeds, while enhancing the radiotherapeutic dose to the cancer cells through Au-mediated radiosensitisation effect.

The synthesis of radiolabeled nanoparticles such as albumin micro- and nanospheres [9] or ^{103}Pd-labeled molecules for targeted therapy [10] require the highest achievable Specific Activity (A_S), defined as the ratio between the activity of the radionuclide of interest and the mass of the sum of all radioactive and stable isotopes of the nuclide [11] (ideally approaching the theoretical carrier free value of $A_S(CF) = 2.76\,GBq{\cdot}\mu g^{-1}$). While for the seeds already in use the specific activity is practically unimportant, the nanomedicine approach involving the synthesis of nanoparticles as nano-seeds or as drug carriers high specific activities have to be achieved and only the radioactive component should be present in the synthesis process. Therefore, a quantitative radiochemical separation of the Pd from the Rh target and its co-produced radionuclides is required which can be achieved by ion-exchange reactions or complexation [12].

Currently, ^{103}Pd is produced in reactors via the ^{102}Pd(n,γ) reaction with a very low A_S or in no-carrier-added form with accelerators using proton induced reactions [13].

Irradiation of pure palladium-102 (enriched from 3.2 % natural abundance to 100 %) to saturation ($t_{irr} \simeq 85$ d) in a nuclear reactor with a flux of $10^{15} \cdot n\,s^{-1} \cdot cm^{-2}$ will lead to about 6.8 % of ^{103}Pd.

The most widely used accelerator production method based on high-flux 18 MeV proton irradiation of a ^{103}Rh target in cyclotrons [14, 15] allows to reach a yield [16] equal to 2.40 GBq·C^{-1} and of 3.25 GBq·C^{-1} if protons of 50 MeV could be used.

The use of a deuteron beam appears to be attractive for the production of several radionuclides since the (d,2n) reaction cross-section in the medium to high mass region is generally higher than that of (p,n) reactions [17]. However, studies on this alternative production methods using deuterons are scarce, and only two studies were reported at the beginning of this research work [18, 19].

The present work presents experimental results for the cross-sections of the ^{103}Rh(d,2n)^{103}Pd reaction and of the co-produced radionuclides in the 5–33 MeV energy range.

2. Experimental

The excitation functions were determined using the stacked-foil technique. Stacks of thin foils consisted of alternating high purity aluminium (as energy degrader and monitor foils inserted between the Rh and the Ti targets), rhodium and titanium foils. In particular each stack was composed of four or five couple of Rh and Al foils, depending on the irradiation energy, and (i) by one Ti foil, inserted as final monitor foil in the stack for the JRC-Ispra irradiations or (ii) one Ti foil after each of the Rh/Al foils in the stack for the GIP-ARRONAX irradiations.

High purity ^{103}Rh targets (99.9 %, Goodfellow Cambridge Ltd., Ermine Business Park, Huntingdon PE29 6WR, UK) had a nominal thickness of 12.5 or 25 μm ($\sim$15.1-31.7 mg·cm^{-2} with a general relative uncertainty of $\pm$2 %: these

values of target thickness used in the calculation were measured accurately by weighing).

Low-energy irradiations were carried out on five stacks with the cyclotron (Scanditronix MC40, K = 38) of the JRC-Ispra at different incident energies covering the energy range from 16.6 MeV down to 5.2 MeV with a constant current of 100 nA for a duration of 1 hour.

Each irradiation was carried out in an insulated target holder under vacuum, which was designed as an elongated Faraday cup to determine the integrated charge of the deuteron beam. Inside the Faraday cup a strong magnet was installed to avoid escaping of scattered or backscattered electrons as the loss of such electrons could lead to a virtually larger deuteron charge on the foil stacks. Two coaxial Al collimators (5 mm in diameter) were placed in front of the Faraday cup. Based on the distance between the collimators and the last couple of quadrupoles, a maximum broadening of the beam of a few μm was calculated. The charge was integrated by a current integrator (BIC Brookhaven Instruments Corporation, Austin, TX, USA; model 1000C), calibrated within 2 % of uncertainty by an authorized calibration service (Nemko S.p.A., Biassono, MB, Italy). The incident deuteron energy had an uncertainty of ± 0.20 MeV [20].

The reliability of the integrated current has been validated by the values of the cross-sections measured for ^{nat}Ti targets used as monitor foils, compared with the IAEA tabulated monitor reaction ^{nat}Ti(d,x)^{48}V [21].

Medium and high-energy irradiations were carried out with an IBA C70 cyclotron of the ARRONAX center, Saint-Herblain (FR). The ARRONAX cyclotron delivers deuteron beams at variable energies with an energy uncertainty of ± 0.25 MeV [22]. The stacks were irradiated with an external deuteron beam. A 75 μm thick kapton foil was used as beam exit window, separating the beam line vacuum from atmospheric pressure in the vault. The stacks were located 68 mm downstream in air.

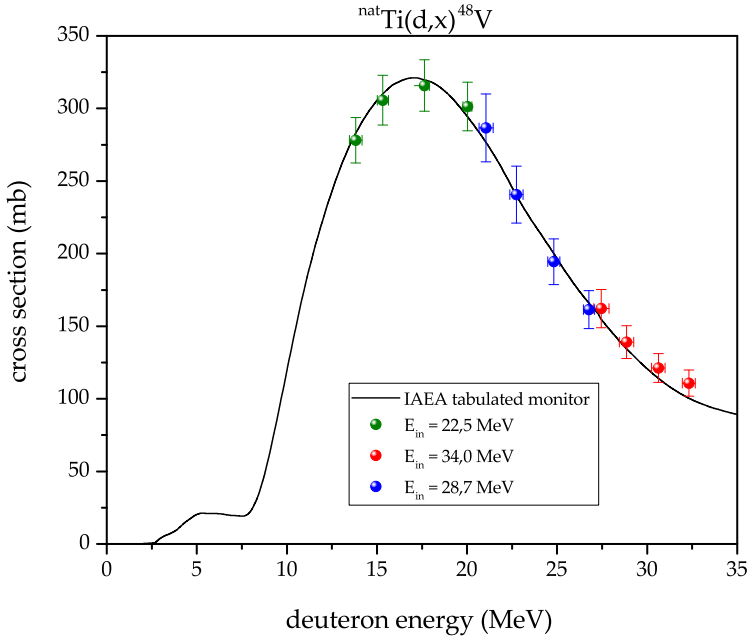

Figure 1: Excitation function for ^{nat}Ti(d,x)^{48}V nuclear reactions.

During the irradiation, an instrumented beam stop was used to control the beam current stability. However, it was not used as a Faraday cup with precise intensity measurements, since it is not under vacuum and is not equipped with a magnet to avoid escaping of scattered or backscattered electrons.

In this case, it was mandatory to use titanium and aluminium foils as degraders and as monitors to determine the experimental beam intensity value and energy from the ^{nat}Ti(d,x)^{48}V and ^{27}Al(d,x)^{24}Na IAEA tabulated monitor reactions [21] (Figures 1 and 2).

Four different stacks were irradiated with a different incident energy in order to minimize energy straggling in a single experiment and to cover the energy range from 34 MeV down to 14 MeV, with an overlap of more than 2 MeV with the irradiations performed at the JRC-Ispra. The irradiations were carried out with a mean beam intensity of about 170 nA for 1 h.

The mean deuteron beam energy and energy degradation in each foil were

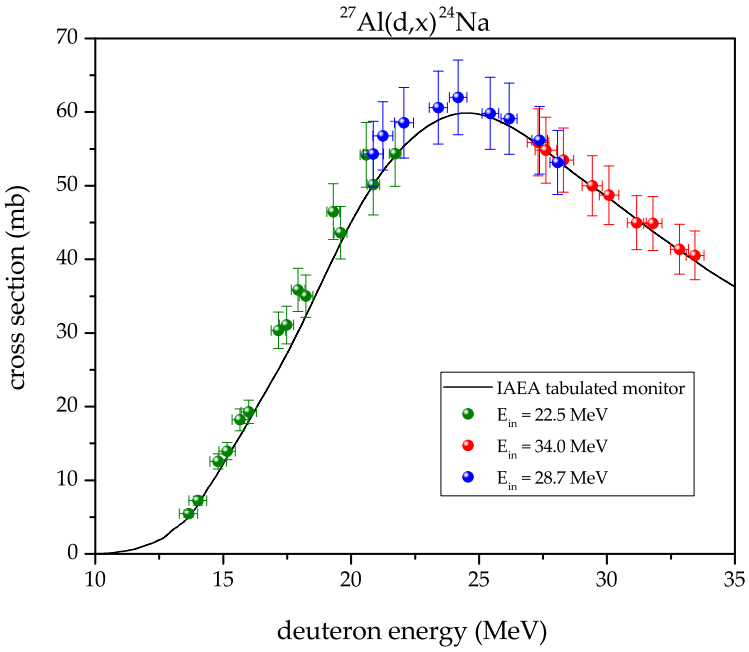

Figure 2: Excitation function for ^{27}Al(d,x)^{24}Na nuclear reactions.

computed by the Monte Carlo based computer code SRIM 2013 [23]. The uncertainty of the mean energy in each foil (± 0.2–0.4 MeV) includes the energy uncertainty of the extracted deuteron beam, as well as the uncertainties (± 0.1–0.3 MeV) in the mean mass thicknesses and the beam-energy straggling inside the target foils.

The activity of the radionuclides detected in each foil was measured at the LASA laboratory (INFN and Physics Dept. of University of Milan, Segrate MI), without any chemical processing, by calibrated high purity germanium (HPGe) detectors (EG&G Ortec, 15 % relative efficiency, FWHM = 2.2 keV at 1.33 MeV). The detectors were calibrated in energy and efficiency with certified ^{152}Eu and ^{133}Ba sources (CercaLEA, France and Amersham, UK). All foils were measured in the same geometrical position as that used for the calibration sources in order to avoid corrections for different geometries. The distance from

the detector cap was sufficiently high to reduce dead time and pile up errors to negligible values ($< 0.1\,\%$). The first measurements of the samples were generally started within a few hours (for the Ispra irradiations) or within 48 hours (for ARRONAX irradiations) after the end of bombardment (EOB). The measurements continued for about six months in order to follow the decay of the main radionuclides and to let completely decay eventual "parent" radionuclides.

The overall uncertainty of the determined cross-sections is caused by several error sources in the measurement and evaluation process. Regarding the measurement process, a typical component is related to the statistical error in the peak counts: particular attention is given to reduce this value as low as possible ($< 1\,\%$–$18\,\%$, depending on the radionuclides and on the energies). Other significant error sources were: the target thickness and uniformity ($< 2\,\%$), the integrated charge ($\leq 2\,\%$), the uncertainty of the calibration sources (1.5 % and 2.0 %) and the fitting of the detector efficiency curves ($< 1\,\%$), with an overall relative error of 4–20 %.

The published data for the abundance of the gamma emissions and the half-lives were considered as being exact. Admittedly, especially the uncertainty of the low values of the abundance of the gamma emission of ^{103}Pd will add directly to the overall error in the determination of the reaction cross section [17]. Decay characteristics for the radionuclides investigated, as summarized in Table 1, were taken from [1] and [24].

3. Results

The thin foils were measured, positioning them on the detector with the beam-on and the detector cup being face to face. The experimental cross-sections σ(E) [cm^2·atom^{-1}] for each target were calculated from the thin-target yield making use of the relationship:

$$\sigma(E) = y_{EOIB}(E) \cdot \frac{M \cdot Z \cdot e \cdot \Delta E}{\lambda \cdot N_A \cdot \rho x} \qquad (1)$$

Table 1: Decay data [1] of Pd, Rh and Ru radionuclides and contributing reactions with the energies E_γ used for the activity calculation and the corresponding abundancies I_γ. The thereshold energy (E_{th}) evaluation is based on the mass defects reported in [24].

Nuclide	$t_{1/2}$	Contributing reactions	E_{th} (MeV)	E_γ (keV)	I_γ (%)
^{104}Pd	stable	^{103}Rh(d,n)^{104}Pd	0		
^{103}Pd	16.991 d	^{103}Rh(d,2n)^{103}Pd	3.62	357.47	0.0221
^{102}Pd	stable	^{103}Rh(d,3n)^{102}Pd	11.39		
^{101}Pd	8.47 h	^{103}Rh(d,4n)^{101}Pd	22.17	296.29	19.2
^{102m}Rh	3.742 a [25]*	^{103}Rh(d,p2n)^{102m}Rh	11.91	697.49	43.9
		^{103}Rh(d,dn)^{102m}Rh	7.91		
		^{103}Rh(d,t)^{102m}Rh	1.53		
^{102g}Rh	207 d	^{103}Rh(d,p2n)^{102g}Rh	11.77	468.59	2.813
		^{103}Rh(d,dn)^{102g}Rh	7.77		
		^{103}Rh(d,t)^{102g}Rh	1.39		
^{101m}Rh	4.34 d	^{103}Rh(d,p3n)^{101m}Rh	19.52	306.85	87
		^{103}Rh(d,d2n)^{101m}Rh	17.25		
		^{103}Rh(d,tn)^{101m}Rh	10.87		
^{101g}Rh	3.3 a	^{103}Rh(d,p3n)^{101g}Rh	19.36	197.6	70.88
		^{103}Rh(d,d2n)^{101g}Rh	17.09		
		^{103}Rh(d,tn)^{101g}Rh	10.71		
^{100g}Rh	20.8 h	^{103}Rh(d,p4n)^{100g}Rh	29.44	539.51	80.6
		^{103}Rh(d,d3n)^{100g}Rh	27.18		
		^{103}Rh(d,t2n)^{100g}Rh	20.80		
^{103}Ru	39.26 d	^{103}Rh(d,2p)^{103}Ru	2.25	497.08	90.9

*The value reported in [1] is $\sim$2.9 a: in this case we prefer to use a more precise value from another database

where $y_{EOIB}(E)$ is the thin-target yield [Bq·C^{-1}·Mev^{-1}] at the End Of Instantaneous Bombardment, M denotes the atomic mass [g·mol^{-1}], N_A Avogadro's constant [atom·mol^{-1}], $E = \langle E \rangle$ denotes the mean deuteron beam energy crossing the "thin" foil [MeV], e the electron charge [C], Z the atomic number of the projectile, ΔE the beam energy loss in the target [MeV], λ the decay constant [s^{-1}] of the investigated radionuclide, and ρx the mass thickness [g·cm^{-2}]. $y_{EOIB}(E)$ was calculated using the equation:

$$y_{EOIB}(E) = \frac{COUNTS_\gamma}{\varepsilon_\gamma \cdot I_\gamma \cdot LT} \cdot \frac{1}{Q \cdot \Delta E} \cdot D(RT) \cdot G(t_{irr}) \cdot e^{\lambda \cdot \Delta t} \tag{2}$$

where Q is the integrated deuteron charge [C], $COUNTS_\gamma$ denotes the net photo-peak counts at energy E_γ above the continuum background, I_γ the γ-emission absolute abundance, ε_γ the experimental efficiency of the HPGe detector at the γ-energy considered, LT the Live counting Time [s], RT the Real counting Time, which is the sum of LT and the Dead counting Time DT (RT =LT + DT [s]), Δt denotes the waiting time from the EOB [s], t_{irr} the irradiation time [s] and ΔE the beam energy loss in the foil [MeV]. The quantities $D(RT)$ (the decay factor to correct decay during counting time) and $G(t_{irr})$ (the growing factor to correct decay during irradiation) with the dimension 1 are defined as:

$$D(RT) = \frac{\lambda \cdot RT}{1 - e^{-\lambda \cdot RT}} \tag{3}$$

and

$$G(t_{irr}) = \frac{\lambda \cdot t_{irr}}{1 - e^{-\lambda \cdot t_{irr}}}. \tag{4}$$

The measured excitation functions are compared in Figures 4–13 with available literature data. The numerical data are collected in Table 2 and Table 3. The cross-sections for Pd isotopes were also theoretically calculated with EMPIRE-3.2.2 [26] in order to evaluate the best energy of irradiation to obtain ^{103}Pd with

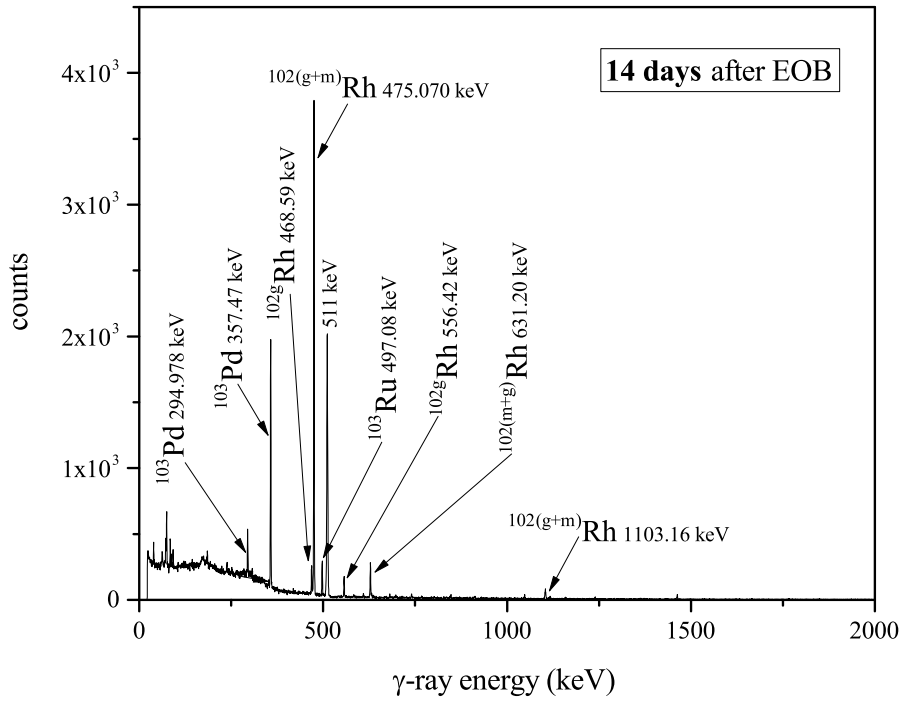

Figure 3: Example of γ-ray spectrum. The counting uncertainty of the 357.47 keV emission is $\sim$ 1.5 %. The γ-ray emissions of ^{103}Pd are clearly visible in spite of their low intensities.

the highest A_S (Section 3.7).

In spite of the differences in the irradiation conditions (see Section 2) there is a very good overlap between the experimental data obtained from the JRC-Ispra and the ARRONAX facilities.

3.1. $^{103}Rh(d,2n)^{103}Pd$

^{103}Pd has a half-life of $t_{1/2}$ = 16.991 d and can be produced by the (d,2n) reaction. The activity was determined from the 357.47 keV emission (I_γ = 0.0221 %). In some cases (e.g. Figure 3), we could verify the activity using the 294.978 keV emission (I_γ = 0.00280 %). The results are in very good agreement and provide some confidence in the tabulated γ-intensities in spite of their small values.

Due to the small γ-ray intensities, which suggest that they may exhibit a

Table 2: Experimental cross-sections (±1 Standard Deviation, ±1SD) of the ^{103}Rh(d,xn)^{103,101}Pd, ^{103}Rh(d,2p)^{103}Ru and ^{103}Rh(d,p5n)^{100g}Rh reactions

Energy (MeV)	^{101}Pd (mb)	^{103}Pd (mb)	^{103}Ru (mb)	^{100g}Rh (mb)
5.2 ± 0.3		22.5 ± 2.9		
6.5 ± 0.3		131.2 ± 7.8	0.0108 ± 0.0016	
7.4 ± 0.2		325 ± 18	0.0204 ± 0.0013	
7.8 ± 0.3		317 ± 21	0.0271 ± 0.0040	
8.4 ± 0.2		516 ± 30	0.0370 ± 0.0031	
8.9 ± 0.3		604 ± 35	0.0513 ± 0.0053	
9.5 ± 0.2		681 ± 41	0.0567 ± 0.0047	
10.0 ± 0.3		800 ± 45	0.0639 ± 0.0054	
10.5 ± 0.2		845 ± 49	0.0780 ± 0.0062	
11.1 ± 0.3			0.0870 ± 0.0047	
11.5 ± 0.3			0.090 ± 0.011	
12.2 ± 0.3			0.1019 ± 0.0063	
12.5 ± 0.3		1166 ± 64	0.1063 ± 0.0063	
13.2 ± 0.4		1127 ± 64	0.1076 ± 0.0055	
13.6 ± 0.3		1141 ± 70	0.1085 ± 0.0069	
13.9 ± 0.3		1253 ± 72	0.1200 ± 0.0063	
14.3 ± 0.3		1140 ± 110	0.125 ± 0.014	
14.5 ± 0.3		1210 ± 110	0.146 ± 0.012	
15.0 ± 0.4		1261 ± 71	0.1491 ± 0.0080	
15.5 ± 0.4		1108 ± 62	0.1404 ± 0.0071	
15.7 ± 0.3		1090 ± 96	0.157 ± 0.013	
16.1 ± 0.4		1127 ± 53	0.196 ± 0.010	
16.5 ± 0.3		1044 ± 93	0.180 ± 0.015	
16.6 ± 0.4		1040 ± 59	0.1747 ± 0.0088	
18.7 ± 0.3		743 ± 66	0.326 ± 0.028	
21.3 ± 0.3		393 ± 66	0.628 ± 0.052	
21.7 ± 0.4		374 ± 37	0.625 ± 0.052	
23.8 ± 0.4		240 ± 28	1.002 ± 0.082	
25.8 ± 0.3	12.3 ± 1.1	208 ± 25	1.37 ± 0.11	
27.7 ± 0.3	56.6 ± 4.7	189 ± 24	1.68 ± 0.14	
28 ± 0.4	46.9 ± 3.9	169 ± 24	1.59 ± 0.13	
29.8 ± 0.4	122 ± 10	143 ± 24	1.92 ± 0.16	0.233 ± 0.031
31.5 ± 0.4	195 ± 16	141 ± 31	2.17 ± 0.18	0.684 ± 0.067
33.1 ± 0.4	266 ± 22	96 ± 20	2.39 ± 0.19	1.36 ± 0.12

Table 3: Experimental cross-sections (±1SD) of the ^{103}Rh(d,pxn)$^{\bullet}$Rh

Energy (MeV)	^{102m}Rh (mb)	^{102g}Rh (mb)	^{101m}Rh (mb)	^{101g}Rh (mb)
7.4 ± 0.2		1.40 ± 0.32		
8.9 ± 0.3		1.91 ± 0.18		
9.5 ± 0.2		2.04 ± 0.18		
10.0 ± 0.3	0.230 ± 0.079	3.35 ± 0.55		
10.5 ± 0.2	0.161 ± 0.064	3.77 ± 0.22		
11.1 ± 0.3	0.66 ± 0.12	7.83 ± 0.47		
12.2 ± 0.3	0.81 ± 0.20	9.69 ± 0.60		
12.5 ± 0.4	0.407 ± 0.055	10.37 ± 0.72		
13.2 ± 0.4	0.51 ± 0.10	11.09 ± 0.53		
13.6 ± 0.3	0.74 ± 0.18	11.0 ± 1.2		
13.9 ± 0.3	0.67 ± 0.08	13.51 ± 0.69		
14.3 ± 0.3	1.56 ± 0.27	14.1 ± 1.4		
15.0 ± 0.4	1.46 ± 0.20	15.40 ± 0.88		
15.5 ± 0.4	1.39 ± 0.11	15.21 ± 0.74		
16.1 ± 0.4	2.35 ± 0.29	16.8 ± 1.0		
16.5 ± 0.3	2.21 ± 0.26	17.6 ± 1.5		
16.6 ± 0.4	2.19 ± 0.16	16.89 ± 0.88		
18.7 ± 0.3	8.22 ± 0.83	23.7 ± 2.1		
21.3 ± 0.3	33.6 ± 2.8	32.7 ± 4.8		
21.7 ± 0.4	35.7 ± 3.0	39.1 ± 3.3	1.074 ± 0.089	0.50 ± 0.13
23.8 ± 0.4	73.0 ± 6.0	63.4 ± 5.3	0.950 ± 0.078	1.08 ± 0.23
25.8 ± 0.3	113.4 ± 9.2	85.1 ± 7.1	17.7 ± 1.6	1.58 ± 0.16
27.7 ± 0.3	148 ± 12	105.0 ± 8.6	76.9 ± 6.6	1.86 ± 0.17
28.0 ± 0.4	138 ± 11	97.4 ± 8.0	64.7 ± 5.6	1.97 ± 0.18
29.7 ± 0.4	167 ± 14	112.8 ± 9.2	114 ± 10	3.85 ± 0.34
31.5 ± 0.4	186 ± 15	119.8 ± 9.8	268 ± 23	7.35 ± 0.66
33.1 ± 0.4	191 ± 16	121.8 ± 9.9	371 ± 32	14.3 ± 1.3

large uncertainty, Sudar et al. [27] based their quantification of ^{103}Pd on the X-ray emissions of ^{103}Pd. More recently Hussain et al. [28] pointed out that also the abundance of the emitted X-rays exhibits an uncertainty of up to 20 % which might require a renormalization of the reaction cross sections derived by Sudar et al. [27]. Additionally, also the quantification via X-rays is not straightforward due to interfering X-ray emissions from co-produced nuclides and due to self-absorption effects [27]. Where our quantification was based on the 357.47 keV and the 294.978 keV emissions both, of which the latter exhibits an even lower intensity, the results agreed very well. This seems to corroborate the statement made by Hussain et al. [28] that the intensity of the 357.4 keV gamma-ray is low but still appears to be correct. Therefore, in the present work we assume that the 357.47 keV and 294.978 keV emissions have an intensity uncertainty of 3.2 % of 2.5 %, respectively [1, 29].

The measured experimental cross-sections are shown in Figure 4 together with the data determined in the earlier studies and curves of theoretical calculations with EMPIRE-II [30], EMPIRE-3.2.2 and TENDL-2015 [31] codes. Our cross-sections are in good agreement with the results of Hermanne et al. [18] (γ data), while they are in the maximum about 15 % higher than those of Ditroi et al. [19]. The prediction of EMPIRE-3.2.2 and EMPIRE-II and the recommended set of Hussain et al. [28] are close to the experimental data, while TENDL-2015 underestimates the reaction cross-sections at energies above 10 MeV.

In order to enable quantitative considerations for the production of ^{103}Pd, it is useful to calculate the Thick-Target Yield (TTY). This was done using the polynomial fit result of the experimental thin-target yields presented in Figure 5 and integrating it up to a given deuteron energy. Figure 6 shows the resulting Thick-Target Yield in comparison with four experimental Thick-Target Yields presented in literature (Dmitrievet al. [32, 33] and Mukhammedov et al. [34]) and the IAEA recommended ones [15] for deuteron (solid line) and proton (dash

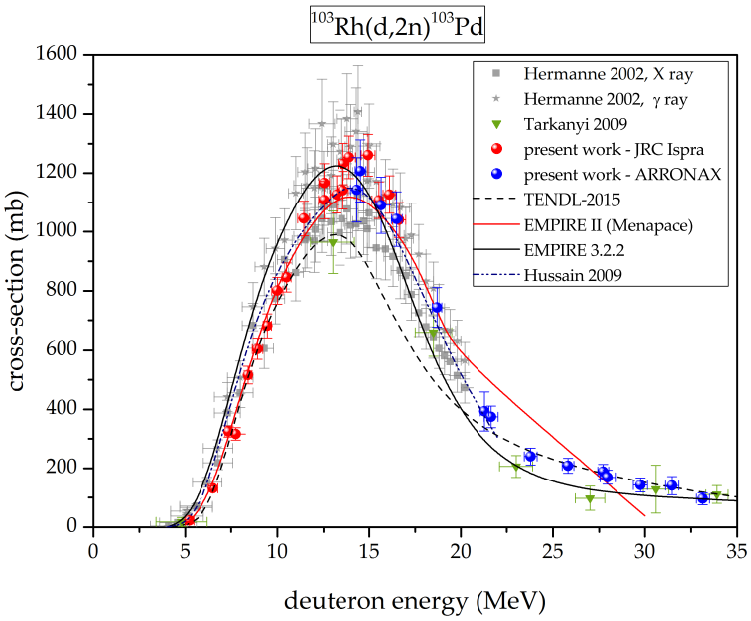

Figure 4: Comparison of the excitation function for the ^{103}Rh(d,2n)^{103}Pd nuclear reaction with literature data and simulation codes.

line) irradiations.

A very good agreement between the experimental data sets and the curve related to the present work can be recognized. The increasing discrepancies between the IAEA curve and the present work at energies above 15 MeV still remain inside the error bars of the experimental data sets.

A comparison between our curve for the deuteron production and the IAEA curve for the proton production of ^{103}Pd shows that the Yields are comparable up to 12 MeV. For higher particle energies the achievable Thick-Target Yield with deuterons is higher than with protons.

3.2. $^{103}Rh(d,4n)^{101}Pd$

^{101}Pd has a half-life of $t_{1/2}$ = 8.47 h and can be produced by the (d,4n) reaction. The activity was assessed through the 296.29 keV gamma line (I_γ = 19.2 %).

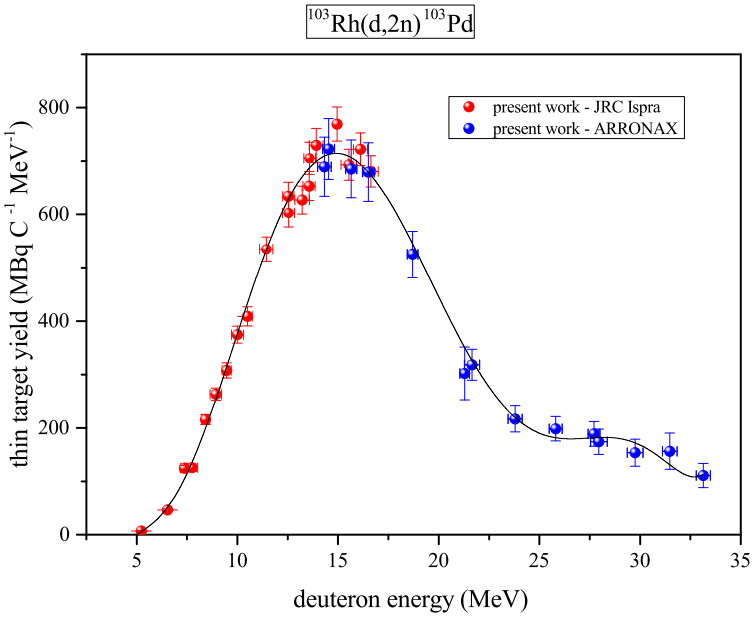

Figure 5: ^{103}Rh(d,2n)^{103}Pd experimental and fitted thin-target yield.

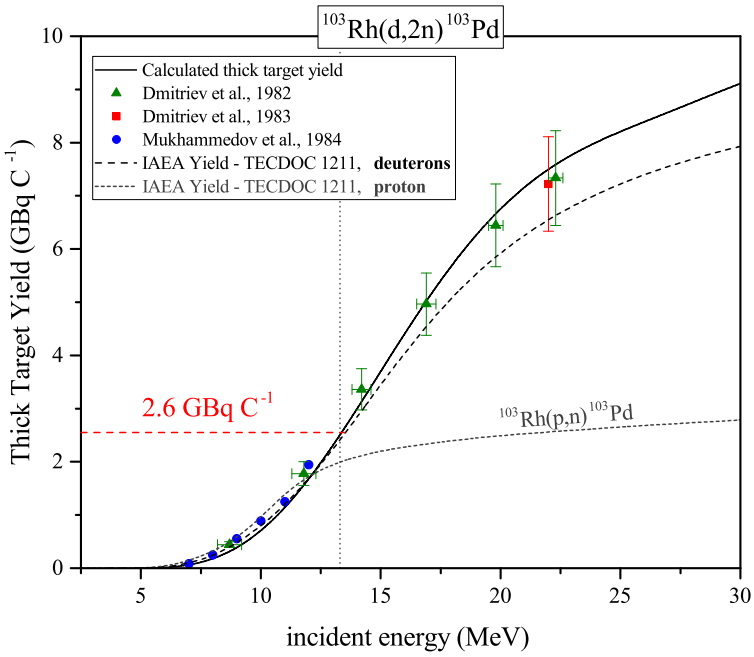

Figure 6: Calculated Thick-Target Yields for the production of ^{103}Pd as a function of deuteron irradiation energy.

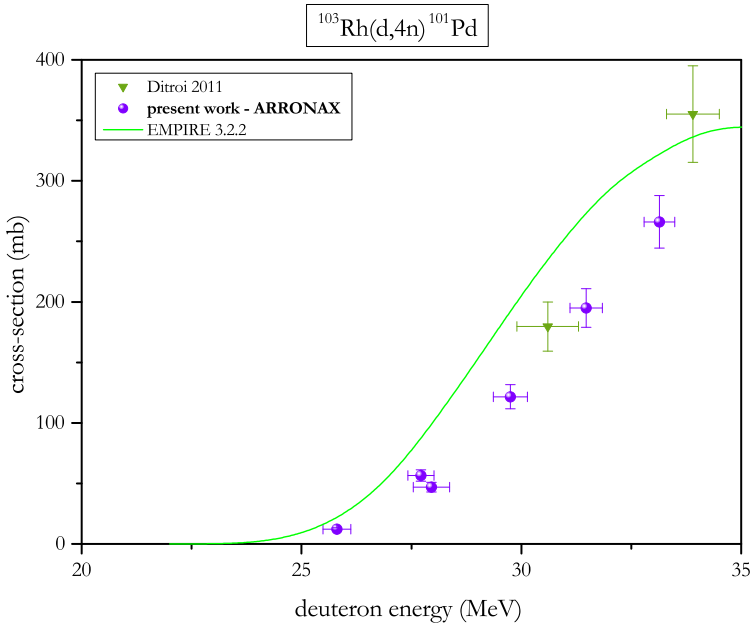

Figure 7: Excitation function for ^{103}Rh(d,4n)^{101}Pd nuclear reaction.

Our cross-sections are in good agreement with the results of Ditroi et al. [19] (Figure 7). The prediction of EMPIRE-3.2.2 is generally higher than experimental values.

3.3. $^{103}Rh(d,x)^{102m,g}Rh$

^{102}Rh can be produced via the (d,p2n), (d,dn) and (d,t) reactions.

^{102m}Rh has a half-life of $t_{1/2}$ = 3.742 a and the activity was assessed through the 697.49 keV gamma line (I_γ = 43.90 %).
Our cross-sections are in reasonable agreement with the results of Ditroi et al. [19] and Hermanne et al. [18] (Figure 8).

^{102g}Rh has a half-life of $t_{1/2}$ = 207 d and its activity was determined from the 468.59 keV gamma line (I_γ = 2.813 %). Under our experimental conditions ^{102g}Rh is mainly formed directly because the contribution of the decay of the

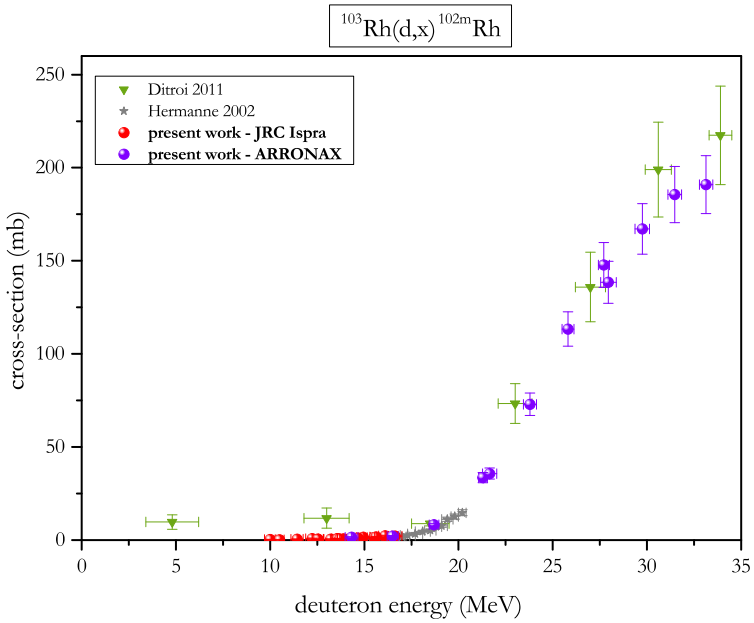

Figure 8: Excitation function for ^{103}Rh(d,x)^{102m}Rh nuclear reactions.

metastable level is negligible (only 0.233 % IT and low ratio between the half-lives).

Our cross-sections are in good agreement with the results of Hermanne et al. [18] (Figure 9). The discrepancy with Ditroi et al. [19] may be explained taking into account that Ditroi et al. used the 628.05 keV gamma line to determine the activity but also ^{102m}Rh contributes to this emission (I_γ = 8.5 %) which may result in an overestimation of the ^{102g}Rh activity. It is possible to appreciate this contribution at energies greater than 18 MeV: it is shown in Figure 8 that the ^{103}Rh(d,x)^{102m}Rh cross-section starts to increase rapidly exceeding this energy value.

3.4. ^{103}Rh(d,x)^{101m,g}Rh

^{101}Rh can be produced by the (d,p3n), (d,d2n) and (d,tn) reactions.

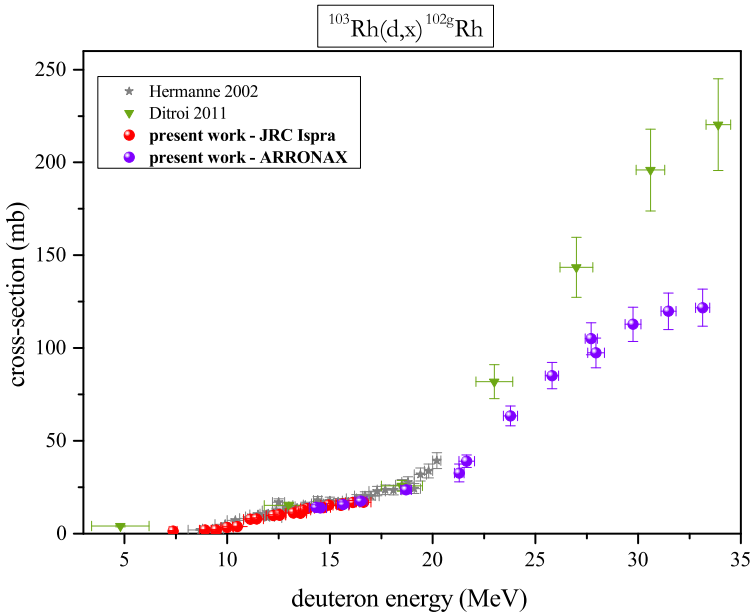

Figure 9: Excitation function for ^{103}Rh(d,x)^{102g}Rh nuclear reactions.

^{101m}Rh has a half-life of $t_{1/2}$ = 4.34 d and the activity was determined from the 306.85 keV emission (I_γ = 87 %); ^{101m}Rh is also formed by the decay of the much shorter lived ^{101}Pd (8.47 h, 99.731 %). Therefore, the measurements for this radionuclide were done once that ^{101}Pd was completely decayed in order to subtract this contribution. Our cross-sections are quite smaller than the results of Ditroi et al. [19] (Figure 10) because Detroi et al. measured the cumulative production of ^{101m}Rh.

^{101g}Rh has a half-life of $t_{1/2}$ = 3.3 a and the activity was determined quantifying the 197.6 keV emission (I_γ = 70.88 %). ^{101g}Rh is also formed by the de-excitation of the shorter lived metastable level ^{101m}Rh and, also in this case, the measurements for this radionuclide were done once that its metastable level was completely de-excited. Our cross-sections are in quite good agreement with the few data points of Ditroi et al. [19] (Figure 11).

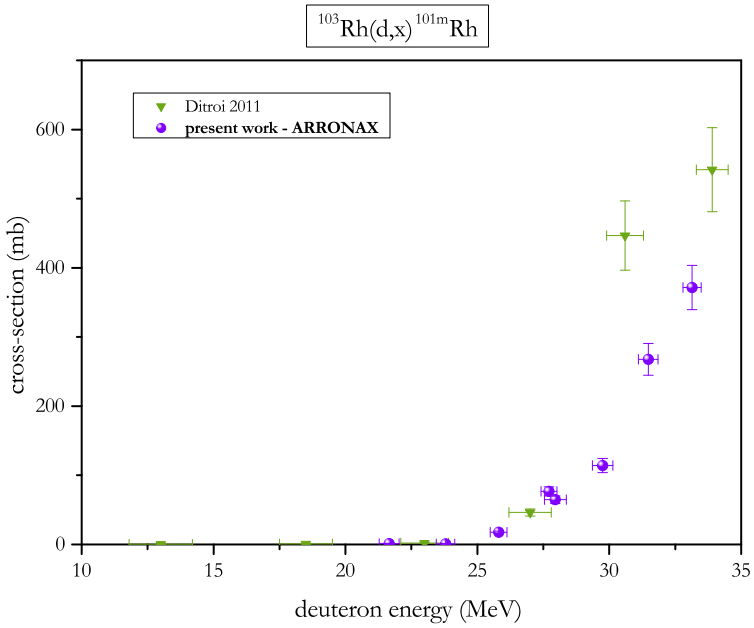

Figure 10: Excitation function for ^{103}Rh(d,x)^{101m,cum}Rh nuclear reactions.

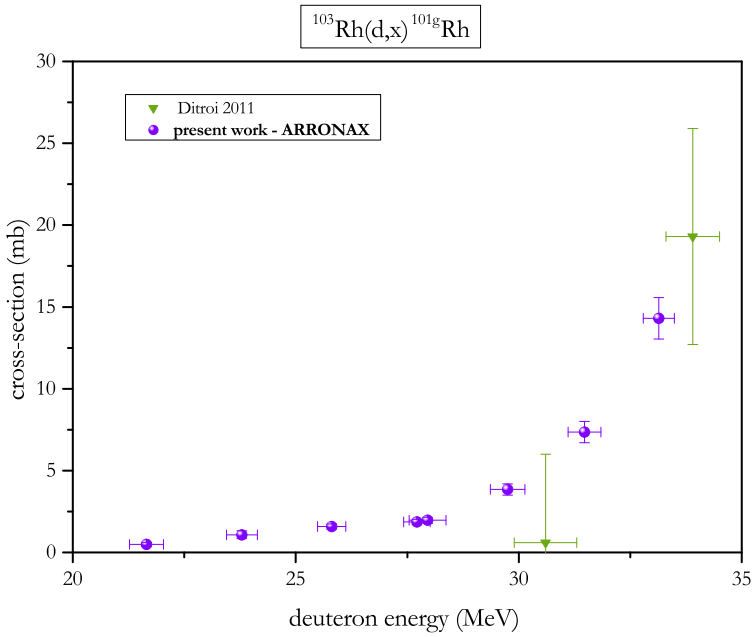

Figure 11: Excitation function for ^{103}Rh(d,x)^{101g}Rh nuclear reactions.

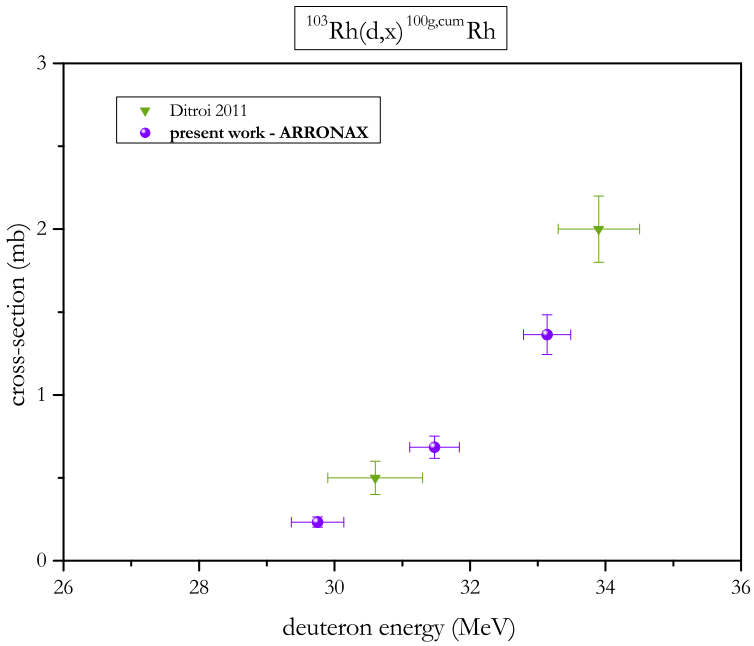

Figure 12: Excitation function for ^{103}Rh(d,x)^{100g,cum}Rh nuclear reactions.

3.5. $^{103}Rh(d,x)^{100g,cum}Rh$

^{100}Rh can be produced by the (d,p4n), (d,d3n) and (d,t2n) reactions.

^{100g}Rh has a half-life of $t_{1/2}$ = 20.8 h and the activity was determined analysing the 539.51 keV gamma emission (I_γ = 80.6 %)

The determined cross-section includes a contribution from the not measured short lived and totally decayed ^{100m}Rh isomer ($t_{1/2}$ = 4.7 m).

The derived cross-section data are in good agreement with the results of Ditroi et al. [19] (Figure 12).

3.6. $^{103}Rh(d,2p)^{103}Ru$

^{103}Ru has a half-life of $t_{1/2}$ = 39.26 d and can be produced via the (d,2p) reaction. The activity was determined from the 497.08 keV gamma emission (I_γ = 90.9 %).

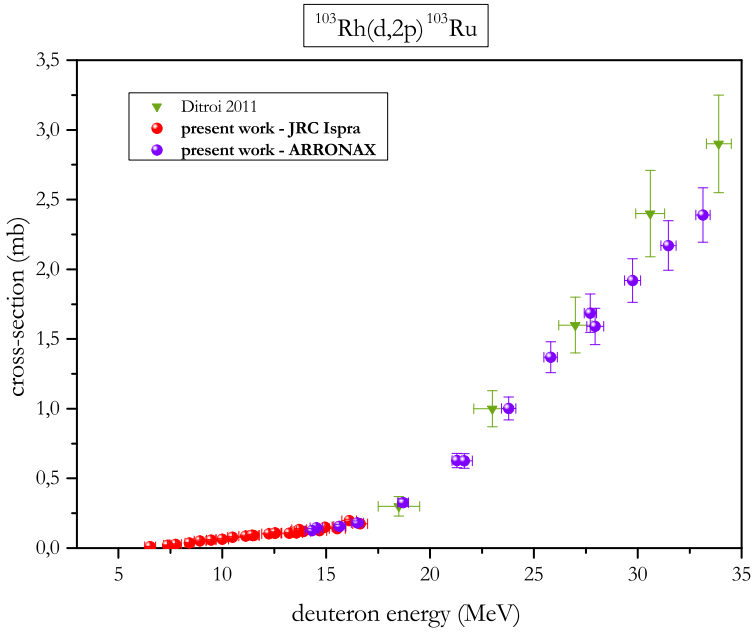

Figure 13: Excitation function for ^{103}Rh(d,2p)^{103}Ru nuclear reaction.

The determined cross-sections are in good agreement with the results of Ditroi et al. [19] (Figure 13).

3.7. Specific Activity for ^{103}Pd production

In spite of the good agreement between the presented experimental data for the production of ^{103}Pd and the theoretical calculations using EMPIRE-3.2.2 code there is a certain uncertainty in the calculation of the stable ^{104}Pd via the (d,n) reaction due to difficulties to incorporate the deuteron breakup process in the simulation codes. However, the uncertainties associated with these difficulties are less for heavier nuclei (such as ^{103}Rh) when compared with light nuclei such as ^{19}F where the effects may be dominating. In any case they are more pronounced for (d,p) reactions [35] and do also contribute up to 50 % to (d,2n) reactions [36] which are in the present case acceptably described by EMPIRE-3.2.2 code. It may therefore be justified to assume that this effect is not critical

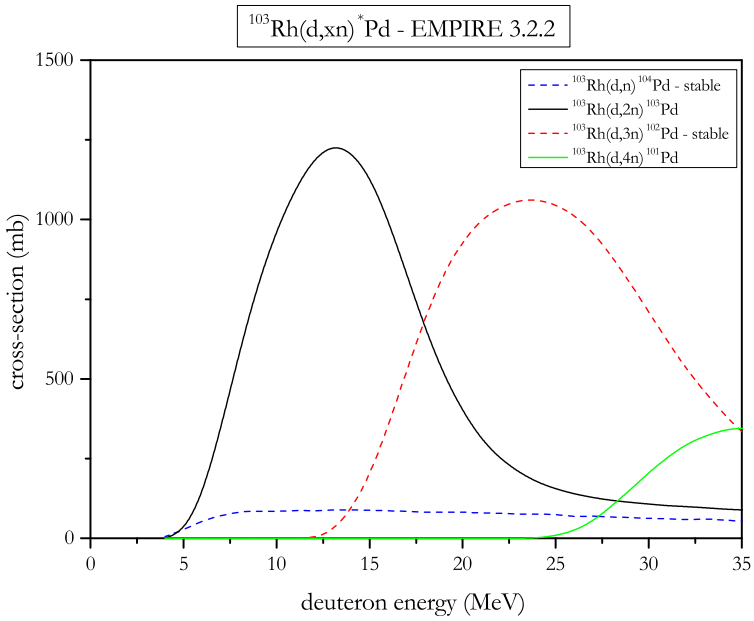

Figure 14: Excitation functions for ^{103}Rh(d,x)$^{\bullet}$Pd nuclear reactions calculated with the model EMPIRE-3.2.2

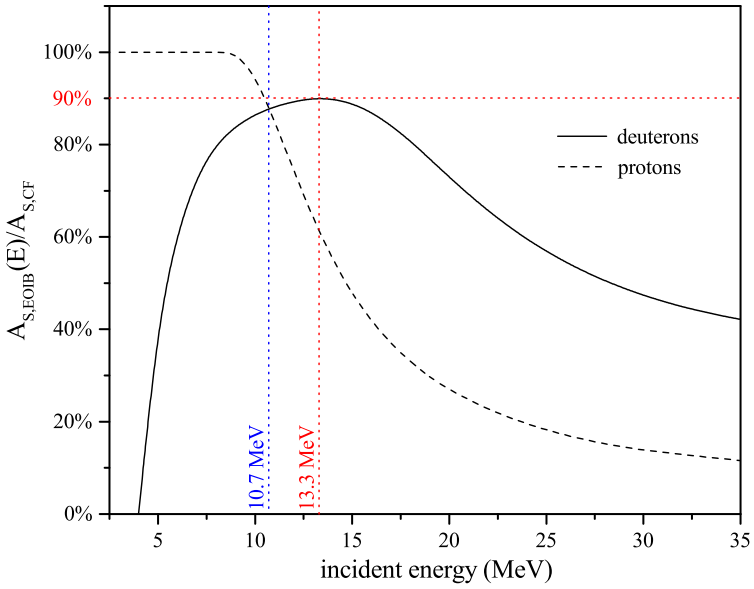

Figure 15: Ratio between the A_S at the End Of an Instantaneous Bombardment and the A_S(CF) calculated from the results presented in Figure 14

for the derivation of the achievable specific activity.

Based on the EMPIRE simulation (Figure 14) and in case of a thick target with total energy absorption, in order to obtain the highest A_S of ^{103}Pd (90 %), the best incident energy is 13.3 MeV (Figure 15). The curve presented in Figure 15 is exact for an Instantaneous Bombardment but, for an incident deuteron energy smaller than 22 MeV (the energy threshold for the production of ^{101}Pd), it is a very good description at the End of Bombardment for $t_{irr} \ll (\lambda_{^{103}Pd})^{-1}$ (i.e. $t_{irr} \ll 588\,h$).

Additionally we calculated the Specific Activity of ^{103}Pd for the production using protons using the cross-section data for the ^{103}Rh(p,n)^{103}Pd nuclear reaction recommended by the IAEA [15] and the cross-section data for the ^{103}Rh(p,xn)^{102,101}Pd nuclear reactions reported in TENDL-2015 [31]

.

Normalizing the calculated Specific Activity at the end of bombardment to its theoretical carrier free value it can be recognized from Figure 15 that for proton energies up to about 8.5 MeV the value of $A_{S,EOIB}/A_S(CF)$ stays at nearly 100 % and drops below the value for deuteron activation when a proton energy of 10.7 MeV is exceeded. Thus, the achievement of higher Thick-Target Yields making use of the ^{103}Rh(p,n)^{103}Pd reaction is compromised above 8.5 MeV proton energy by the achievable specific activity and drops above 10.7 MeV below the values for the specific activity that can be obtained with deuterons.

It should be noted that a co-production of Rh and Ru isotopes does not compromise the radiochemical purity as these elements can be separated from Pd easily [12].

4. Conclusions

In the present study the excitation functions for the radionuclides produced by cyclotron irradiation of Rh targets with deuteron beams have been experimentally determined in the energy range from 5 to 33 MeV. In particular, the cross-section for ^{103}Pd production by ^{103}Rh(d,2n)^{103}Pd nuclear reactions have been determined.

In the energy range presented here, the only radio-isotopic impurity is the ^{101}Pd radionuclide that has an energy threshold of 22 MeV and an half-life of 8.47 h.

In order to achieve a high Specific Activity A_S it is mandatory to take into account also the production of stable palladium isotopes (cf. Figure 15). The presented excitation curves allow the calculation of the optimized ^{103}Pd batch yield and Specific Activity. For deuteron activations using the ^{103}Rh(d,2n)^{103}Pd reaction the highest specific activity can be achieved with an incident deuteron energy of 13.3 MeV, and it is possible to produce 2.6 GBq C^{-1} of ^{103}Pd at the EOIB. The same product quality can be obtained by proton irradiations making use of the ^{103}Rh(p,n)^{103}Pd reaction with an incident proton energy of about 10.5 MeV however at the expense of an about 3 times lower Thick-Target Yield (see Figure 6). This could be compensated by a combination of higher proton beam current and longer irradiation time. Unfortunately, at least at the moment, the number of cyclotrons that can provide deuterons with an energy above 13 MeV (taking into account losses in beam entrance windows etc.) is very limited.

The radiochemical separation of the ^{103}Pd from the target material is easier the smaller the target mass, which points to deuterons having a higher stopping power than protons and hence a shorter range in the target material. For 13.3 MeV deuterons a thick target would correspond to a 188 μm thick Rh foil. Comparing this with the optimized irradiation conditions for protons we have to compare with the range of 10.5 MeV protons in Rh which requires a thickness of about 214 μm to slow the protons to the energy threshold for the production of

^{103}Pd. Therefore, no decisive advantage can be derived from this consideration. However, using a proton energy around 17 to 18 MeV, which is the maximum for many cyclotrons used in medical environments, a thick Rh target needs to have a thickness of at least 500 μm and only about 30 % of the theoretical specific activity can be obtained.

So, the use of deuteron beams leading to high TTYs, high radionuclidic purity, high specific activity is accompanied by the co-production of a small amount of rhodium to be removed by the radiochemical separation. Due to larger $-dE/dx$ in the case of deuteron more ^{103}Pd is formed when compared over proton irradiations which reduces the required mass of ^{103}Rh for the targets: this is the major advantage of using deuteron beams because of the high cost of the high pure rhodium targets.

The main issue with the production of ^{103}Pd by deuteron irradiations is the scarce availability of cyclotrons providing high deuteron energies with reasonable intensity. But due to the not so short half-life of ^{103}Pd radionuclide, nothing prevents to produce it now and in future in adequate Centres.

Acknowledgements

This work was funded by the Italian National Institute of Nuclear Physics (INFN) in the framework of the research project TECHN-OSP (CSN5).

Special thanks to the whole staff of the cyclotron of the Institute for Health and Consumer Protection, JRC-Ispra, EC: this was the last work together after years of very good researches and results.

References

[1] R. B. Firestone, C. M. Baglin, S. Y. F. Chu, Table of Isotopes: 1999 Update with CD-ROM, 1999 Update, 8th Edition, Wiley-Interscience, 1999.

[2] National Nuclear Data Center, National Nuclear Data Center, information extracted from the NuDat
http://www.nndc.bnl.gov/nudat2/, accessed: 2016-11-21 (2016).
URL http://www.nndc.bnl.gov/nudat2/

[3] Y. Yoshioka, Current status and perspectives of brachytherapy for prostate cancer, International Journal of Clinical Oncology 14 (1) (2009) 31–36. doi:10.1007/s10147-008-0866-z.

[4] J. P. Pignol, B. Keller, E. Rakovitch, R. Sankreacha, H. Easton, W. Que, First report of a permanent breast ^{103}Pd seed implant as adjuvant radiation treatment for early–stage breast cancer, International Journal of Radiation Oncology*Biology*Physics 64 (1) (2006) 176 –181. doi:10.1016/j.ijrobp.2005.06.031.

[5] E. Semenova, P. T. Finger, Palladium-103 radiation therapy for small choroidal melanoma, Ophthalmology 120 (11) (2013) 2353–2357. doi:10.1016/j.ophtha.2013.04.017.

[6] E. Lechtman, N. Chattopadhyay, Z. Cai, S. Mashouf, R. Reilly, J. Pignol, Implications on clinical scenario of gold nanoparticle radiosensitization in regards to photon energy, nanoparticle size, concentration and location, Physics in Medicine and Biology 56 (15) (2011) 4631–4647, cited By 75. doi:10.1088/0031-9155/56/15/001.

[7] B. L. Jones, S. Krishnan, S. H. Cho, Estimation of microscopic dose enhancement factor around gold nanoparticles by Monte Carlo calculations, Medical Physics 37 (7) (2010) 3809–3816. doi:10.1118/1.3455703.

[8] S. Moeendarbari, R. Tekade, A. Mulgaonkar, P. Christensen, S. Ramezani, G. Hassan, R. Jiang, O. K. Öz, Y. Hao, X. Sun, Theranostic nanoseeds for efficacious internal radiation therapy of unresectable solid tumors, Scientific Reports 6 (2016) 20614. doi:10.1038/srep20614.

[9] V. M. Petriev, V. K. Shiryaev, V. G. Skvortsov, L. A. Smakhtin, O. Y. Kochnov, O. A. Smoryzanova, Pharmacokinetics of a new radiopharma-

ceutical based on alubmin microspheres and palladium-103 and modified by heat and radiation, Pharmaceutical Chemistry Journal 45 (8) (2011) 449–453. doi:10.1007/s11094-011-0652-5.

[10] A. R. Jalilian, M. Sadeghi, Y. Yari-Kamrani, M. R. Ensaf, Development of [^{103}pd]-2-acetylpyridine 4n-methyl thiosemicarbazone complex for targeted therapy, Journal of Radioanalytical and Nuclear Chemistry 268 (3) (2006) 605–611. doi:10.1007/s10967-006-0212-8.

[11] J. J. M. de Goeij, M. L. Bonardi, How do we define the concepts specific activity, radioactive concentration, carrier, carrier-free and no-carrier-added?, Journal of Radioanalytical and Nuclear Chemistry 263 (1) (2005) 13–18. doi:10.1007/s10967-005-0004-6.

[12] F. L. Bernardis, R. A. Grant, D. C. Sherrington, A review of methods of separation of the platinum-group metals through their chlorocomplexes, Reactive and Functional Polymers 65 (3) (2005) 205–217. doi:10.1016/j.reactfunctpolym.2005.05.011.

[13] R. A. Kuznetsov, V. M. Radchenko, V. A. Tarasov, N. N. Andreichuk, L. S. Lebedeva, V. D. Gavrilov, A. N. Pakhomov, Production techniques and quality control of sealed radioactive sources of palladium-103, iodine-125, iridium-192 and ytterbium-169 – IAEA-TCDOC-1512, INTERNATIONAL ATOMIC ENERGY AGENCY, 2006, Ch. Principles development of ^{103}Pd reactor production technology and palladium seed core production technology by electrochemical plating, pp. 128–142.

[14] INTERNATIONAL ATOMIC ENERGY AGENCY, Cyclotron Produced Radionuclides: Physical Characteristics and Production Methods, no. 468 in Technical Reports Series, INTERNATIONAL ATOMIC ENERGY AGENCY, Vienna, 2009.

[15] F. Tárkányi, S. M. Qaim, M. Nortier, R. Capote, A. Ignatyuk, B. Scholten, S. F. Kovalev, B. Kiraly, E. Menapace, Y. N. Shubin, Nuclear Data for the

Production of Therapeutic Radionuclides, INTERNATIONAL ATOMIC ENERGY AGENCY, 2011, Ch. Charged particle production of ^{64,67}Cu, ^{67}Ga, ^{86g}Y, ^{102}Rh, ^{103}Pd, ^{111g,114m}In, ^{124,125}I, ^{169g}Yb, ^{177g}Lu, ^{186g}Re, ^{192g}Ir, ^{210,211}At and ^{225}Ac, pp. 143–376.

[16] N. Otuka, S. Takács, Definitions of radioisotope thick target yields, Radiochimica Acta 103 (1) (2015) 1–6. doi:10.1515/ract-2013-2234.

[17] S. M. Qaim, Nuclear data for production and medical application of radionuclides: Present status and future needs, Nuclear Medicine and Biology 44 (2017) 31–49. doi:http://dx.doi.org/10.1016/j.nucmedbio.2016.08.016.

[18] A. Hermanne, M. Sonck, S. Takács, F. Tárkányi, Y. Shubin, Study on alternative production of ^{103}Pd and characterisation of contaminants in the deuteron irradiation of ^{103}Rh up to 21 MeV, Nuclear Instruments and Methods in Physics Research Section B: Beam Interactions with Materials and Atoms 187 (1) (2002) 3–14. doi:10.1016/S0168-583X(01)00851-5.

[19] F. Ditrói, F. Tárkányi, S. Takács, A. Hermanne, H. Yamazaki, M. Baba, A. Mohammadi, A. V. Ignatyuk, Study of activation cross-sections of deuteron induced reactions on rhodium up to 40 MeV, Nuclear Instruments and Methods in Physics Research Section B: Beam Interactions with Materials and Atoms 269 (18) (2011) 1963–1972. doi:10.1016/j.nimb.2011.05.026.

[20] C. Birattari, M. Castiglioni, M. Silari, Absolute calibration of accelerator beam energies by the crossover technique, Nuclear Instruments and Methods in Physics Research Section A: Accelerators, Spectrometers, Detectors and Associated Equipment 320 (3) (1992) 413–431. doi:10.1016/0168-9002(92)90938-Z.

[21] F. Tárkányi, S. Takács, K. Gul, A. Hermanne, M. G. Mustafa, M. Nortier, P. Obložinský, S. M. Qaim, B. Scholten, Y. N. Shubin, Z. Youxiang, Beam

monitor reactions, in: Charged Particle Cross-Section Database for Medical Radioisotope Production: Diagnostic Radioisotopes and Monitor Reactions, INTERNATIONAL ATOMIC ENERGY AGENCY, 2001, pp. 49–152.

[22] F. Haddad, L. Ferrer, A. Guertin, T. Carlier, N. Michel, J. Barbet, J.-F. Chatal, ARRONAX, a high-energy and high-intensity cyclotron for nuclear medicine, European Journal of Nuclear Medicine and Molecular Imaging 35 (7) (2008) 1377–1387. doi:10.1007/s00259-008-0802-5.

[23] J. F. Ziegler, M. D. Ziegler, J. P. Biersack, SRIM - the stopping and range of ions in matter (2010), Nuclear Instruments and Methods in Physics Research, Section B: Beam Interactions with Materials and Atoms 268 (11-12) (2010) 1818–1823. doi:10.1016/j.nimb.2010.02.091.

[24] M. Wang, G. Audi, A. H. Wapstra, F. G. Kondev, M. MacCormick, X. Xu, B. Pfeiffer, The Ame2012 atomic mass evaluation 36 (12) (2012) 1603. doi:10.1088/1674-1137/36/12/003.

[25] J. K. Tuli, Nuclear Wallet Cards, 8th Edition, NNDC, Brookhaven National Laboratory, 2011.
URL http://www.nndc.bnl.gov/wallet/wall35.pdf

[26] M. Herman, R. Capote, B. Carlson, P. Obložinský, M. Sin, A. Trkov, H. Wienke, V. Zerkin, EMPIRE: Nuclear reaction model code system for data evaluation, Nucl. Data Sheets 108 (2007) 2655. doi:10.1016/j.nds.2007.11.003.

[27] S. Sudár, F. Cserpák, S. M. Qaim, Measurements and nuclear model calculations on proton-induced reactions on ^{103}Rh up to 40 MeV: evaluation of the excitation function of the ^{103}Rh(p,n)^{103}Pd reaction relevant to the production of the therapeutic radionuclide ^{103}Pd, Applied Radiation and Isotopes 56 (6) (2002) 821 – 831. doi:10.1016/S0969-8043(02)00054-4.

[28] M. Hussain, S. Sudár, M. N. Aslam, H. A. Shah, R. Ahmad, A. A. Malik, S. M. Qaim, A comprehensive evaluation of charged-particle data for production of the therapeutic radionuclide ^{103}Pd, Applied Radiation and Isotopes 67 (10) (2009) 1842–1854. doi:10.1016/j.apradiso.2009.06.010.

[29] D. De Frenne, Nuclear data sheets for A = 103, Nuclear Data Sheets 110 (9) (2009) 2081 – 2256. doi:10.1016/j.nds.2009.08.002.

[30] E. Menapace, M. L. Bonardi, F. Groppi, E. Persico, Z. B. Alfassi, Experimental and calculated nuclear reaction data relevant to innovative production of medical radioisotopes, in: Proc. Intern. Conf. Nuclear Data for Science and Technology, Vol. 2, EDP Sciences, 2008, pp. 1403–1406. doi:10.1051/ndata:07655.

[31] A. J. Koning, D. Rochman, Modern nuclear data evaluation with the TALYS code system, Nuclear Data Sheets 113 (12) (2012) 2841–2934. doi:10.1016/j.nds.2012.11.002.

[32] P. P. Dmitriev, M. V. Panarin, G. A. Molin, Production of ^{103}Pd by the ^{103}Rh(p, n) and ^{103}Rh(d, 2n) reactions, At.Energ. 53 (1982) 198.

[33] P. P. Dmitriev, N. N. Krasnov, G. A. Molin, Yields of radioactive nuclides formed by bombardment of a thick target with 22-MeV deuterons, Tech. Rep. INDC(CCP)-210/L, INTERNATIONAL ATOMIC ENERGY AGENCY (1983).
URL http://www.iaea.org/inis/collection/NCLCollectionStore/_Public/15/043/15043227.p

[34] S. Mukhammedov, A. Vasidov, E. Pardaev, Use of proton and deuteron activation methods of analysis in the determination of elements with Z > 42, At.Energ. 56 (1984) 50.

[35] J. P. Farrell Jr., C. M. Vincent, N. Austern, Three-body model of deuteron breakup and stripping, Annals of Physics 96 (2) (1976) 333–381. doi:10.1016/0003-4916(76)90195-0.

[36] M. Avrigeanu, V. Avrigeanu, Deuteron breakup effects on activation cross sections at low and medium energies, Journal of Physics: Conference Series 205 (1) (2010) 012014. doi:10.1088/1742-6596/205/1/012014.